Characterization of the EGF-Like Module Pair 3-4 from Vitamin K-Dependent Protein S Using NMR Spectroscopy Reveals Dynamics on Three Separate Time Scales and Extensive Effects from Calcium Binding†

Andreas Muranyi,*,‡ Johan Evenäs,‡,§ Yvonne Stenberg,||,⊥ Johan Stenflo,|| and Torbjörn Drakenberg‡

Physical Chemistry 2, Lund University, P.O. Box 124, S-221 00 Lund, Sweden and Clinical Chemistry, Lund University, University Hospital, Malmö, S-205 02 Malmö, Sweden

Received February 28, 2000; Revised Manuscript Received September 27, 2000

ABSTRACT: Protein S, a cofactor of anticoagulant activated protein C, exhibits three high-affinity Ca^{2+}-binding sites in a region comprising four EGF modules. The EGF 3-4 module pair constitutes the smallest fragment that retains one high-affinity Ca^{2+}-binding site and is therefore useful for investigation of the structural basis of the unusually high-affinity Ca^{2+} binding compared to other EGF-containing proteins characterized so far. Extensive chemical shift effects caused by Ca^{2+} binding to the EGF 3-4 module pair are observed, particularly from Ca^{2+} binding to the high-affinity site in EGF 4. Ca^{2+} binding to the high-affinity site in EGF 4 and the low-affinity site in EGF 3 is associated with slow and fast exchange on the NMR time-scale, respectively. We show the presence of two isoforms, characterized by a cis or trans Lys 167−Pro 168 peptide bond, that do not convert on time scales that were accessible to the experiments ($k_{ex} < 0.2\ s^{-1}$). Both conformers have similar Ca^{2+} affinities and backbone dynamics. Further, broadening of ^1H resonances involving residues in the major β-sheet of EGF 3 and ^{15}N exchange terms, primarily in the N-terminal part of the protein, indicate the presence of slow exchange on a microsecond to millisecond time scale. ^{15}N spin relaxation data suggest that the module pair has a well-defined relative orientation between EGF modules 3 and 4 and has a significantly anisotropic rotational diffusion tensor in solution.

Protein S (reviewed in ref *1*) is a vitamin K-dependent protein that acts as a cofactor to the anticoagulant activated protein C (APC).[1] APC cleaves and inactivates factor Va and factor VIIIa, which are cofactors of factor Xa (FXa) and factor IXa (FIXa), respectively (the "a" denotes the activated form of a cofactor or enzyme). Protein S consists of an N-terminal Gla module followed by a region sensitive to cleavage by thrombin and FXa followed by four EGF modules and a C-terminal module that is homologous to a steroid-hormone-binding protein in plasma (*2*−*4*). EGF modules are characterized by six cysteine residues that form disulfide bonds in a pattern 1−3, 2−4, and 5−6. A subset of EGF modules bind Ca^{2+} and has a consensus sequence Asp/Asn-Xxx-Asp/Asn-Glu/Gln N-terminal of the first Cys and Xxx-Asn/Asp-$(Xxx)_4$-Tyr/Phe between the third and fourth Cys (*5*−*7*). The three C-terminal EGF modules of protein S have the sequence motif associated with Ca^{2+} binding. It has been shown that protein S contains four high-affinity Ca^{2+}-binding sites with dissociation constants (K_d) in the range 10 nM-1 μM and that the Ca^{2+}-free form is more susceptible to proteolysis (*8*). Protein S deficiency as well as functionally deficient protein S, due to point mutations in the protein S gene, is associated with an increased risk for thrombotic disease (*1*, *9*). Some of these mutations occur in the EGF region, and a subset of these involve Ca^{2+}-ligating residues.

In previous studies, single EGF modules from protein S have been synthesized, and recombinant proteins consisting of two, three, or four out of the four EGF modules have been produced (*10*, *11*). In EGF 1-4, EGF 2-4, and EGF 1-3, up to three Ca^{2+}-binding sites with K_ds in the nanomolar to micromolar range were found. However, the isolated EGF 3 (pS EGF 3) and EGF 4 (pS EGF 4) modules each had a K_d in the millimolar range. It is apparent that the Ca^{2+} affinity is strongly dependent on the presence of neighboring modules (Figure 1). It has previously been demonstrated for FIX and FX that the Ca^{2+} affinity of an EGF module increases 10−20-fold when a neighboring Gla module is added N-terminally (*12*, *13*). Similar results were observed in EGF module pairs from fibrillin-1. The affinity for Ca^{2+} binding increased 70-fold when Ca^{2+}-binding (cb) EGF 13 was

† This work was supported by grants from the Swedish Foundation of Strategic Research, the Swedish Medical Research Council and the European Union Biotechnology Program (Contract BIO4-CT96-0662). Some of the NMR experiments were run at the Swedish NMR Center.

* To whom correspondence should be addressed. E-mail: andreas.muranyi@fkem2.lth.se. Fax: +46-46-222 45 43. Phone: +46-46-222 82 07.

‡ Physical Chemistry 2.

§ Present address: Departments of Medical Genetics and Biochemistry, Medical Sciences Building, University of Toronto, Toronto, Ontario, M5S 1A8, Canada.

|| Clinical Chemistry.

⊥ Present address: BioInvent Therapeutic AB, Sölvegatan 41, S-223 70 Lund, Sweden.

[1] Abbreviations: 1D, one-dimensional; 2D, two-dimensional; APC, activated protein C; cb, Ca^{2+} binding; CPMG, Carr-Purcell-Meiboom-Gill; CSA, chemical shift anisotropy; DSS, 2,2-dimethyl-2-silapentane-5-sulfonic acid; EGF, epidermal growth factor; FX, factor X; FXa, activated factor X; HSQC, heteronuclear single-quantum coherence; Hya, *erythro*-β-hydroxyaspartic acid; Hyn, *erythro*-β-hydroxyasparagine; NOESY, nuclear Overhouser enhancement spectroscopy; pS, protein S; TB, transforming growth factor β (TGF-β) binding protein-like; TOCSY, total correlation spectroscopy.

10.1021/bi0004450 CCC: $19.00
Published on Web 11/29/2000

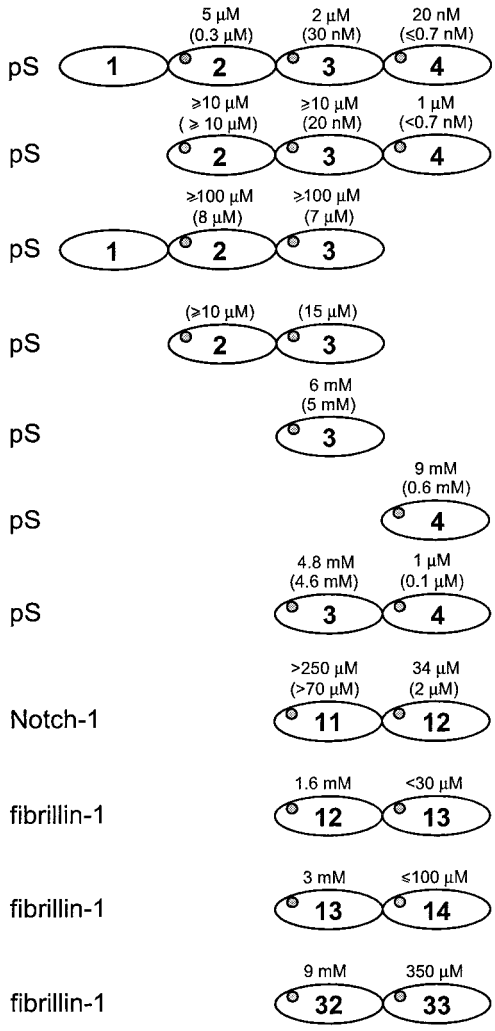

FIGURE 1: Summary of K_d values for Ca^{2+} binding in the absence (in parentheses) or the presence of 150 mM NaCl to a number of constructs investigated by us and others. High affinity Ca^{2+} binding [in EGF 1-4, EGF 2-4, and EGF 1-3 of protein S (pS)] has been measured with Ca^{2+} chelator methods using UV spectroscopy (*65*). The low affinity Ca^{2+} binding found in isolated modules EGF 3 and EGF 4 and in the module pair EGF 2-3 were determined using 1D ^{1}H NMR (*10*, *65*). The K_d of the low-affinity site of EGF 3 and the high-affinity site of EGF 4 in pS EGF 3-4 has been measured by monitoring the Ca^{2+} titration with 2D ^{1}H-^{15}N HSQC experiments and the Ca^{2+} chelator method, respectively, this study and (*21*). The K_d for Ca^{2+} binding to Notch-1 EGF 11-12 was determined using the chelator method (*22*). The Fibrillin-1 cbEGF 12-13, cbEGF 13-14, and cbEGF 32-33 module pairs were investigated using 2D NOESY experiments and intrinsic fluorescence (*14*, *23*, *25*).

preceded by its N-terminal neighbor (*14*). In the cbEGF 32-33 pair from fibrillin-1 the C-terminal module had 25-fold higher Ca^{2+} affinity than the N-terminal module (*15*). In contrast, the Ca^{2+} affinity was only modestly higher in the TB-cbEGF 32 module pair from fibrillin-1 than in the isolated cbEGF 32 module (*16*, *17*). However, in another heterologous module pair, the CUB-EGF module pair from complement protease C1r, the Ca^{2+} affinity was 300-fold higher than in the isolated EGF module (*18*−*20*). Protein S exhibits the highest Ca^{2+} affinities and the largest increases in Ca^{2+} affinities induced by adding neighboring modules found so far. In the EGF 3-4 module pair from protein S (pS EGF 3-4), the affinity of the N-terminal site is similar in the pair (K_d = 4.8 mM) and in the isolated module (K_d = 6.1 mM), whereas the Ca^{2+} affinity of EGF 4 is almost 4 orders of magnitude higher in the module pair (K_d = 1 μM) than it is in the isolated module (K_d = 8.6 mM) (*10*, *21*).

Although the affinity of EGF 4 for Ca^{2+} in pS EGF 3-4 is significantly lower than it is for this module in the larger constructs or the entire protein S molecule, this affinity is higher than what is observed for the C-terminal module in several other EGF module pairs from other proteins. The affinity of EGF 4 in pS EGF 3-4 is between 9 and 30-fold higher than the high-affinity site of cbEGF 12-13 from fibrillin-1, 34-fold stronger than that of Notch EGF 11-12, up to 100-fold stronger than that of fibrillin-1 cbEGF 13-14 and 350-fold higher than reported for the C-terminal site in cbEGF 32-33 from fibrillin-1 (Figure 1) (*14*, *15*, *22*, *23*). A sequence comparison of some of these EGF-module pairs does not give a clear-cut explanation to the differences (Figure 2). In protein S EGF 4, the consensus Ca^{2+} motif is preceded by an additional negatively charged residue (Glu 201) which replaces a hydrophobic residue in the sequences mentioned above and might contribute to the free energy of ion binding without being a Ca^{2+} ligand (*24*). However, such an amino acid change is not expected to give such a dramatic effect on the affinity (*12*). It is also possible that the amino acids that form the hydrophobic cluster, which mediates the module−module interaction, are important factors for the increase in affinity. This contact was observed in the structure of fibrillin-1 cbEGF 32-33 (*25*). It involves residues, which in pS EGF 3-4 correspond to Tyr 191 in the last loop of EGF 3 and Pro 219 and Gly 220 in the hairpin turn of the major β-sheet of EGF 4.

In this paper, we present a detailed characterization of pS EGF 3-4 using homo- and heteronuclear multidimensional NMR techniques. Structural heterogeneity, characterized by double sets of resonances for several residues in EGF 3, was discovered. ^{1}H-^{15}N HSQC experiments were employed to monitor the effects of Ca^{2+} binding to all residues in pS EGF 3-4 and the dissociation constants for Ca^{2+} binding to the N-terminal binding site were calculated for both structural forms. Finally, ^{15}N spin relaxation experiments were applied to address questions relating to chemical exchange, diffusional anisotropy, and structural rigidity.

EXPERIMENTAL PROCEDURES

Protein Production. The production of pS EGF 3-4 as well as pS EGF 3 has been described in detail elsewhere (*10*, *21*). In brief, pS EGF 3-4 was expressed in *Escherichia coli* BL21(DE3) pLysS cells as a fusion protein with a His-tag. ^{15}N-Labeling was achieved by expression in minimal medium containing $^{15}NH_4Cl$ (99.1 at. % ^{15}N). The recombinant protein was reduced and refolded in vitro, correctly folded material was purified and the His-tag removed by proteolytic cleavage. Ca^{2+}-free pS EGF 3-4 was lyophilized and characterized by SDS−PAGE, reversed-phase HPLC, amino acid composition, and immunoblotting using a monoclonal antibody that recognizes a conformation-dependent epitope. Agarose gel electrophoresis in the presence and absence of Ca^{2+} was used as a means of detecting correctly folded Ca^{2+}-binding recombinant pS EGF 3-4. Mass spectroscopy indicated a homogeneous protein with expected molecular mass (9843 Da). Also judging by N-terminal sequencing, the module pair was homogeneous. Besides two N-terminal amino acids

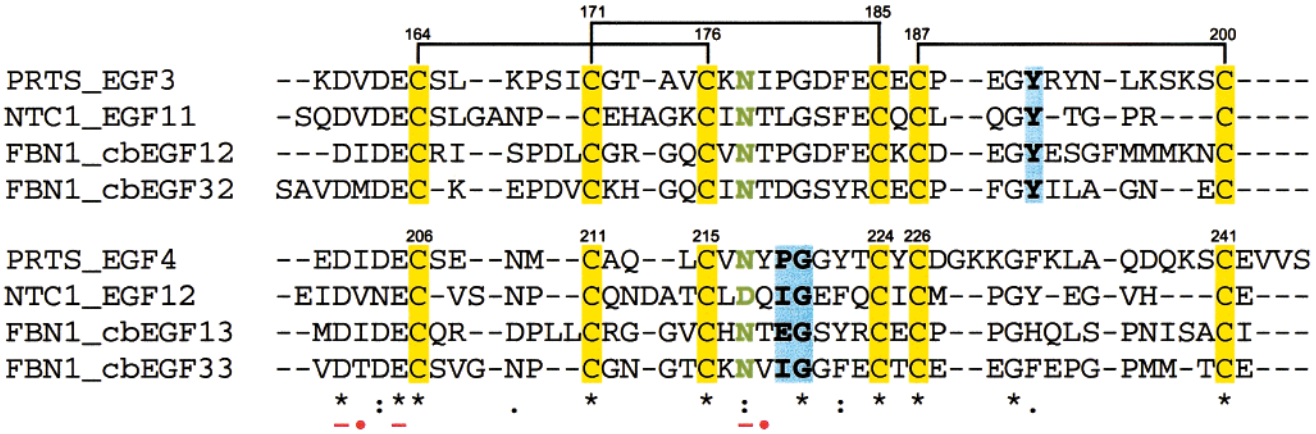

FIGURE 2: Multiple sequence alignment of protein S (PRTS) EGF 3-4, Notch-1 (NTC1), EGF 11-12, and fibrillin-1 (FBN1) Ca^{2+}-binding EGF 12-13 and 32-33 (all sequences are from human). All 12 cysteine residues (yellow and labeled by residue numbering of protein S) are involved in disulfide bonds in a pattern characteristic for EGF modules (indicated by connecting lines). Residues corresponding to those involved in the inter-module hydrophobic cluster in fibrillin-1 cbEGF 32-33 are indicated by blue (*25*). Asn and Asp β-hydroxylated to Hyn and Hya, respectively, in the wild-type proteins are indicated by boldface characters in green. Black symbols indicate the degree of amino acid similarity; (*) identical, (:) very similar, and (.) similar. Red symbols indicate Ca^{2+} ligands observed in fibrillin-1 cbEGF 32-33 and proposed for the other proteins; (−) carboxylate, and (.) carbonyl oxygen. The alignment was made with CLUSTAL W, using BLOSUM weight matrixes and the gap opening penalty and gap extension penalty turned down to 1 and 0.0125, respectively.

originating from the His-tag, His 157 and Met 158, the sequence of the final product comprised residues 159−245 of human protein S.

The EGF 3 module, residues Lys 159−Ile 203, was synthesized using Fmoc chemistry on a Milligen/Biosearch 9050 peptide synthesizer. The peptide was deprotected, cleaved from the resin, extracted, and dried. Thereafter, the peptide was purified by HPLC performed under reducing conditions. Fractions with correct sequence and amino acid composition were refolded as described (*10*) and thereafter purified by reversed-phase HPLC. Amino acid analysis, N-terminal sequencing, and electrospray mass spectrometric analysis gave expected results.

In pS EGF 3-4 as well as in pS EGF 3, the *erythro*-β-hydroxyasparagine (Hyn) residue in position 178 was replaced by Asn, as was the Hyn residue in position 217 of pS EGF 3-4. It has been shown previously that altering the *erythro*-β-hydroxyaspartic acid (Hya) residue to Asp in the homologous position of isolated N-terminal EGF modules of FIX and FX does not significantly change the Ca^{2+} affinity (*26*).

NMR Experiments. All NMR experiments were performed on a Varian Unity Inova with a magnetic field corresponding to a proton frequency of 599.89 MHz. Inverse or triple-resonance probes equipped with pulsed field gradient coils in the Z-direction were used. The experiments were performed at 36 °C with the ^1H carrier set to the water frequency and the ^{15}N carrier to 117.35 ppm except were otherwise stated. Processing was made using FELIX97 (Molecular Simulations Inc., San Diego). ^1H chemical shifts were referenced to DSS at 0.00 ppm, and ^{15}N shifts were indirectly referenced using the frequency ratio $\omega_N/\omega_H = 0.101\ 329\ 118$ (*27*). Spectral analysis was performed with FELIX97 or XEASY (*28*).

Very Slow Exchange. To probe for exchange between major and minor conformations, a heteronuclear correlation experiment (R1EX) was run (*29*). Temperature and exchange delay were varied as follows: 36 °C (738 ms), 41 °C (738 ms), 46 °C (738 ms), 51 °C (738 ms), 56 °C (200 and 738 ms), 61 °C (738 ms), 66 °C (401 ms), and 70 °C (145 ms). The spectra were acquired with 64 transients and 32 (41, 51, and 61 °C) or 64 (36, 46, 56, 66, and 70 °C) complex data points in the t_1 dimension and 1024 complex points in t_2. These experiments were run on a 600 μL ~0.2 mM ^{15}N-labeled sample of the $(Ca^{2+})_1$ form of pS EGF 3-4 at pH 6.0 with 0.1 mM NaN_3 and 1 mM DSS in a 5 mm NMR tube. Integral ratios between peaks in major and minor forms were calculated from volumes measured in ^1H-^{15}N HSQC spectra with 1 and 61 mM $CaCl_2$ from the titration series for the $(Ca^{2+})_1$ and $(Ca^{2+})_2$ states, respectively (see below).

Isolated EGF 3 Module. A total of 5.9 mg of lyophilized pS EGF 3 was dissolved in 600 μL of 90% H_2O/10% D_2O, containing 0.1 mM NaN_3 and 1 mM DSS, yielding a protein concentration of approximately 2 mM. The pH was adjusted to 6.0. Two-dimensional (2D) ^1H NOESY (*30*), with mixing times of 80 and 150 ms, and TOCSY (*31*), with 40 and 110 ms DIPSI isotropic mixing times, were acquired. The spectra were acquired with 96 transients and 300 and 1024 complex data points in the t_1 and t_2 dimensions, respectively. Quadrature detection was implemented using the States-TPPI method (*32*). Spectral width in both dimensions was 6400 Hz. The 40 ms TOCSY and 150 ms NOESY experiments were repeated at 20 and 10 °C to disentangle spectral overlap.

Ca^{2+} Titration. Ca^{2+} binding to pS EGF 3-4 was monitored by titrating 2−4 μL aliquots of 0.060−3.00 M $CaCl_2$ to a 600 μL sample in a 5 mm NMR tube which initially contained 1.1 mM ^{15}N-labeled pS EGF 3-4, 15 ± 1 μM Ca^{2+}, 0.1 mM NaN_3, and 1 mM DSS at pH 6.0.

The Ca^{2+} and protein concentrations in the sample prior to the titration were measured using high-resolution inductively coupled plasma mass spectrometry and acid hydrolysis followed by amino acid analysis, respectively.

The titration was monitored by sensitivity-enhanced gradient selection ^1H-^{15}N HSQC experiments (*33*) employing water flip-back pulses (*34*). Spectral widths were 1700 and 6400 Hz in t_1 and t_2, respectively. Each experiment was run with eight transients and 128 and 1024 complex data points in the t_1 and t_2 dimensions, respectively. A recycle delay of

1.3 s resulted in a recording time of 52 min/spectrum. Twenty-one spectra were recorded, with Ca^{2+} concentrations of 15 μM to 61 mM. At every fifth titration point the pH was measured and, when necessary, adjusted.

Determination of Dissociation Constants. The K_ds of the low-affinity Ca^{2+}-binding site in pS EGF 3-4 and the amide ^1H and ^{15}N chemical shifts δ_{Ca1} and δ_{Ca2} for the $(Ca^{2+})_1$ and $(Ca^{2+})_2$ states, respectively, of the major and minor conformers were determined by employing a simulated annealing procedure (*35*). We simultaneously fitted these parameters to observed chemical shifts from several residues at each Ca^{2+} concentration. Only residues with combined chemical shift changes, $\Delta\delta_{1H\&15N} = \sqrt{\Delta\delta_{1H}{}^2+(\Delta\delta_{15N}/5)^2} > 0.125$ ppm were included in the calculations [$\Delta\delta_{1H}$ and $\Delta\delta_{15N}$ are the shift differences between the $(Ca^{2+})_1$ and $(Ca^{2+})_2$ states for ^1H and ^{15}N amide shifts, respectively]. The following equation was minimized,

$$\sum_{i}^{21}\sum_{j}^{X}[\delta_{Ca1}(j)p_{Ca1}(i) + \delta_{Ca2}(j)p_{Ca2}(i) - \delta_{OBS}(i,j)]^2 \quad (1)$$

where p_{Ca1} and p_{Ca2} are the relative populations of the $(Ca^{2+})_1$ and $(Ca^{2+})_2$ forms, respectively, at Ca^{2+} concentration i, calculated from the protein concentration and the K_d; $\delta_{OBS}(i,j)$ is the observed chemical shift of nuclei j at Ca^{2+} concentration i; X is the total number of nuclei used for the calculation. Data from 21 titration points were included in the calculations. The shifts of the first and last point in the titration were used as initial input values for δ_{Ca1} and δ_{Ca2} while the starting value for K_d was varied. In each round of calculations 10 000 sets of K_d, δ_{Ca1}, and δ_{Ca2} were generated randomly, centered around the input value, and eq 1 was evaluated. The set of input values yielding the lowest residual was retained as initial input values for the next round of calculations. In each new round, the allowed ranges for the randomly selected input values were reduced. The reduction of input ranges continued until the change in the lowest residual from one round to the next was lower than a predefined threshold value. Finally, the K_d value was increased from the calculated value, and the deviation that doubled the residual was taken as a measure of the uncertainty.

The three Ca^{2+} states referred to in the text have the following percentage populations of pS EGF 3-4 with zero, one, or two bound Ca^{2+}, respectively: "$(Ca^{2+})_0$ state" (98.5, 1.5, 0); "$(Ca^{2+})_1$ state" (1, 99, 0); "$(Ca^{2+})_2$ state" (0, 7, 93). These populations were calculated from the protein concentration and the K_d values.

^{15}N Spin Relaxation Experiments. A 600 μL sample of ~0.5 mM ^{15}N-labeled pS EGF 3-4, 0.5 mM Ca^{2+}, 0.1 mM NaN_3, and 1 mM DSS at pH 6.0 was used for all ^{15}N spin relaxation experiments. ^{15}N longitudinal (R_1) and transverse (R_2) relaxation rate constants and {^1H}-^{15}N heteronuclear nuclear Overhauser enhancements (NOE) were measured using 2D gradient-selected sensitivity-enhanced experiments (*36*−*38*) as described (*39*). Longitudinal (η_z) and transverse (η_{xy}) cross-correlation relaxation rate constants resulting from ^1H-^{15}N dipolar and ^{15}N chemical shift anisotropy (CSA) relaxation interference were measured (*40*, *41*). For all experiments, spectral widths were 1700 and 6400 Hz in t_1 and t_2, respectively, and 150 and 1024 complex points were acquired in t_1 and t_2, respectively. ^{15}N decoupling during acquisition employed the GARP-1 decoupling sequence with a field strength of 0.88 kHz (*42*). Sixteen transients per t_1 increment were accumulated in the R_1 and R_2 experiments. The recycle delay between transients was 1.5 and 3.0 s for R_1 and R_2 experiments, respectively. To eliminate effects of interference between ^1H-^{15}N dipolar and ^{15}N CSA relaxation in the R_1 and R_2 experiments, ^1H 180° pulses were applied during the relaxation delays (*43*−*45*). In the CPMG pulse train of the R_2 experiment, the ^{15}N refocusing pulses were applied with a field strength of 4.2 kHz and were separated by a 0.9 ms delay (*46*, *47*). R_1 values were determined by fitting of single exponential decays to the relaxation data given by the peak intensities derived from 10 spectra with eight delays of 11 (*2), 121, 200, 287, 398, 530, 740 (*2), and 1093 ms. Similarly, R_2 values were obtained from 11 spectra with nine delays of 16 (*2), 32, 48, 65, 97, 113, 162 (*2), 226, and 404 ms. The heteronuclear NOE was determined as the ratio of the steady-state intensities measured in two spectra recorded with (NOE) and without (control) a ^1H presaturation period of 4 s. ^1H saturation was achieved with the use of 120° ^1H pulses applied every 5 ms. The recycle delay was 6 s for the control experiment and 2 s prior to the presaturation period for the NOE experiment. The NOE and control experiments were recorded in an interleaved fashion and performed in duplicate. The cross-correlation relaxation rates, η_z and η_{xy}, were measured in pairs of experiments recording coherences mediated by cross-relaxation or autorelaxation. A total of 48 and 16 transients was accumulated for each increment of the former and latter experiments, respectively. The longitudinal cross-correlation relaxation rates, η_z, were determined using eight spectra with six delays of 110 (*2), 150, 190, 230 (*2), 270, and 310 ms. The transverse cross-correlation relaxation rates, η_{xy}, were obtained using seven spectra with five delays of 40 (*2), 60, 80, 100 (*2), and 120 ms. A recycle delay of 2 s was employed in the cross-correlation experiments. The rate constants, η_z, and η_{xy}, were obtained by fitting the function $\tanh(\Delta\eta_i)$, where Δ is the relaxation delay and η_i is the rate constant, against the set of ratios of cross-peak intensities that represent the cross-relaxation and the auto-relaxation, respectively (*40*, *41*).

The relaxation rate constants for a nucleus can be expressed as functions of the power spectral density function $J(\omega)$ at different frequencies (*48*)

$$R_1 = (d^2/4)[J(\omega_H - \omega_N) + 3J(\omega_N) + 6J(\omega_H + \omega_N)] + c^2J(\omega_N) \quad (2)$$

$$R_2 = (d^2/8)[4J(0) + J(\omega_H - \omega_N) + 3J(\omega_N) + 6J(\omega_H) + 6J(\omega_H + \omega_N)] + (c^2/6)[3J(\omega_N) + 4J(0)] + R_{ex} \quad (3)$$

$$\eta_z = -\sqrt{3}cdP_2(\cos\beta)J(\omega_N) \quad (4)$$

$$\eta_{xy} = -(\sqrt{3}cdP_2(\cos\beta)/6)[4J(0) + 3J(\omega_N)] \quad (5)$$

$$\sigma_{NH} = (d^2/4)[6J(\omega_H + \omega_N) - J(\omega_H - \omega_N)] \quad (6)$$

where $d = \mu_0 h\gamma_N\gamma_H\langle r_{NH}{}^{-3}\rangle/8\pi^2$; $c = \gamma_N B_0\Delta\sigma/\sqrt{3}$; μ_0 is the permeability of free space; h is Planck's constant; γ_N and γ_H are the gyromagnetic ratios of ^1H and ^{15}N, respectively;

r_{NH} is the distance between the two nuclei; B_0 is the static magnetic field strength; $\Delta\sigma$ is the axially symmetrical CSA; $P_2(x) = (3x^2 - 1)/2$ is the second-order Legendre polynomial; β is the angle between the symmetry axis of the chemical shift tensor and the bond vector; R_{ex} represents chemical exchange contributions to R_2. The heteronuclear cross-relaxation rate σ_{NH} is related to the steady-state NOE by

$$\mathrm{NOE} = 1 + (\sigma_{NH}/R_1)(\gamma_H/\gamma_N) \quad (7)$$

The exchange-free transverse relaxation rate $R_{2,0}$ can be derived as (*41*)

$$R_{2,0} = [\eta_{xy}/\eta_z(R_1 - 1.249\sigma_{NH}) + 1.079\sigma_{NH}] \quad (8)$$

Equation 8 has the advantage that due to the η_{xy}/η_z ratio, $R_{2,0}$ is derived independently of $\Delta\sigma$ and β. However, for protonated proteins, there is a concern that η_z is affected by cross relaxation between $^1H^N$ and other ^1H spins, particularly in β-sheets, the $^1H^\alpha$ of the preceding residue is close in space to the $^1H^N$ spin and this effect is therefore predicted to be considerable (*44*, *49*). Recently, several papers have been published in which $\Delta\sigma$ and β in biological macromolecules have been quantified using high-resolution NMR spectroscopy (*50*−*52*). This allows the determination of $R_{2,0}$ independently of η_z. By combining eq 5 above and eq 20 in Kroenke et al. (*41*) we derived the following expression,

$$R_{2,0} = (R_2 - 1.079\sigma_{NH}) - R_{ex} = \left(\frac{d^2}{8} + \frac{c^2}{6}\right)\frac{6\eta_{xy}}{\sqrt{3}cdP_2(\cos\beta)} \quad (9)$$

In the calculation of $R_{2,0}$ and R_{ex}, we used $\Delta\sigma = -172 \pm 13$ ppm and $\beta = 18°$ (*50*, *52*). The variation in $\Delta\sigma$ was taken into account by including the difference between the maximal ($\Delta\sigma = -185$) and minimal ($\Delta\sigma = -159$) values of $R_{ex} = R_2 - R_{2,0}$ in the squared error sum.

Estimate of Anisotropy of Diffusion Tensor. Woessner derived expressions for the power spectral density function $J(\omega)$ for cases of an isotropic, axially symmetric, and fully anisotropic rotational diffusion tensor (*53*). In the case of an axially symmetric diffusion tensor the spectral density is described by,

$$J(\omega) = \sum_{j=1}^{3} A_j \frac{\tau_j}{1 + \omega^2 {\tau_c}^2} \quad (10)$$

where $\tau_1^{-1} = 6D_\perp$, $\tau_2^{-1} = 5D_\perp + D_{||}$, $\tau_3^{-1} = 2D_\perp + 4D_{||}$, $A_1 = (3\cos^2\theta - 1)^2/4$, $A_2 = 3\sin^2\theta\cos^2\theta$, $A_3 = (^3/_4)\sin^4\theta$, and θ is the angle between the H−N bond of the residue under consideration and the unique axis of the principal frame of the diffusion tensor. If the structure of the molecule is known the local diffusion constant D_i can be fit to yield the rotational diffusion tensor (*54*, *55*). The structural coordinates of pS EGF 3-4 are not known. Instead, to get an estimate of the anisotropy of the diffusion tensor we calculated theoretical ranges of R_1 and R_2 for $0 < \theta < 90°$ for a number of $D_{||}/D_\perp$ values assuming an axially symmetric diffusion tensor and compared these with the range of experimentally derived R_1 and $R_{2,0}$ values for residues with NOE > 0.7.

Exchange Broadening. In the limits of fast exchange the contribution to the line width ($\Delta\nu_{1/2}$) from Ca^{2+} exchange can be calculated as

$$\Delta\nu_{1/2} = \frac{4\pi(p_{Ca1})^2 p_{Ca2}\delta\nu^2}{k_{off}} \quad (11)$$

where $\delta\nu$ is the chemical shift difference in hertz between the $(Ca^{2+})_1$ and $(Ca^{2+})_2$ states.

RESULTS

Double Sets of Resonances. The sequential assignment of the resonances is described in detail elsewhere (*56*). During the assignment process of pS EGF 3-4, it became evident that many of the amino acid residues in EGF 3 exhibited two sets of resonances. In a ^1H-^{15}N HSQC spectrum of pS EGF 3-4 with equimolar concentration of Ca^{2+}, we observed 124 peaks instead of the expected 99 (Figure 3B). As the sequential assignment was worked through, we noticed the occurrence of sequentially connected fragments that were doubling already unambiguously assigned regions of the protein. We identified 23 cases in which two sets of backbone amide resonances could be assigned to the same residue (Lys 159−Lys 167, Ser 169, Thr 173−Cys 176, Ile 179, Gly 181−Cys 187, Cys 200). Differences in side-chain shifts were also seen for most of these residues. In addition, the side-chain NH_2 shifts of Asn 178 as well as the H^β, H^γ, and H^δ shifts of Pro 168 appear in pairs, consistent with a major and a minor conformation. Interestingly, the chemical shifts of the resonances from pS EGF 3 were very similar to those of pS EGF 3-4, including the shifts of both the major and minor components of doubled spin systems (*56*).

In both the $(Ca^{2+})_1$ and $(Ca^{2+})_2$ states, the intensity ratio between signals from the major and minor forms is approximately 2:1. The shift difference between the major and minor peaks ($\delta_{MAJOR} - \delta_{MINOR}$) varies (Figure 4) with the largest differences seen for Glu 163 to Lys 167. The largest shift difference for each type of nucleus is in the $(Ca^{2+})_1$ state found for Glu 163 H^α (−0.75 ppm), Lys 167 H^N (−0.76 ppm), and Lys 167 N (−2.6 ppm), and in the $(Ca^{2+})_2$ state for Cys 164 H^α (−0.44 ppm), Leu 166 H^N (0.69 ppm), Lys 167 H^N (−0.66 ppm), and N (−3.1 ppm). For several of the double sets of resonances, the chemical shift difference between the two sets changed upon Ca^{2+} binding to the site in EGF 3 (Figure 4). For a few of the resonances emanating from N-terminal residues (Lys 159 and Asp 160), the two sets of resonances coalesce at high Ca^{2+} concentrations. The opposite is seen for Gly 181, Glu 184, and Cys 200, which display only one set of resonances in the $(Ca^{2+})_0$ and $(Ca^{2+})_1$ forms but two sets at elevated Ca^{2+} concentrations. The behavior of Cys 200 is interesting as it is located 13 residues C-terminal of the penultimate residue with double sets of chemical shifts, Cys 187, but connected to this residue via a disulfide bond (Figures 2 and 4). This implies that Ca^{2+} binding to a site, which is located N-terminally in the EGF 3 module, confers a structural rearrangement experienced by the last residue of this module, which is only separated by the one-residue linker (Glu 201) from the first Ca^{2+} ligand in the next module. Although modest, this shift effect is, to our knowledge, the first structural evidence in EGF-module pairs of influence of Ca^{2+}-binding to the site in the N-terminal module on a residue close to the binding site in the C-terminal module.

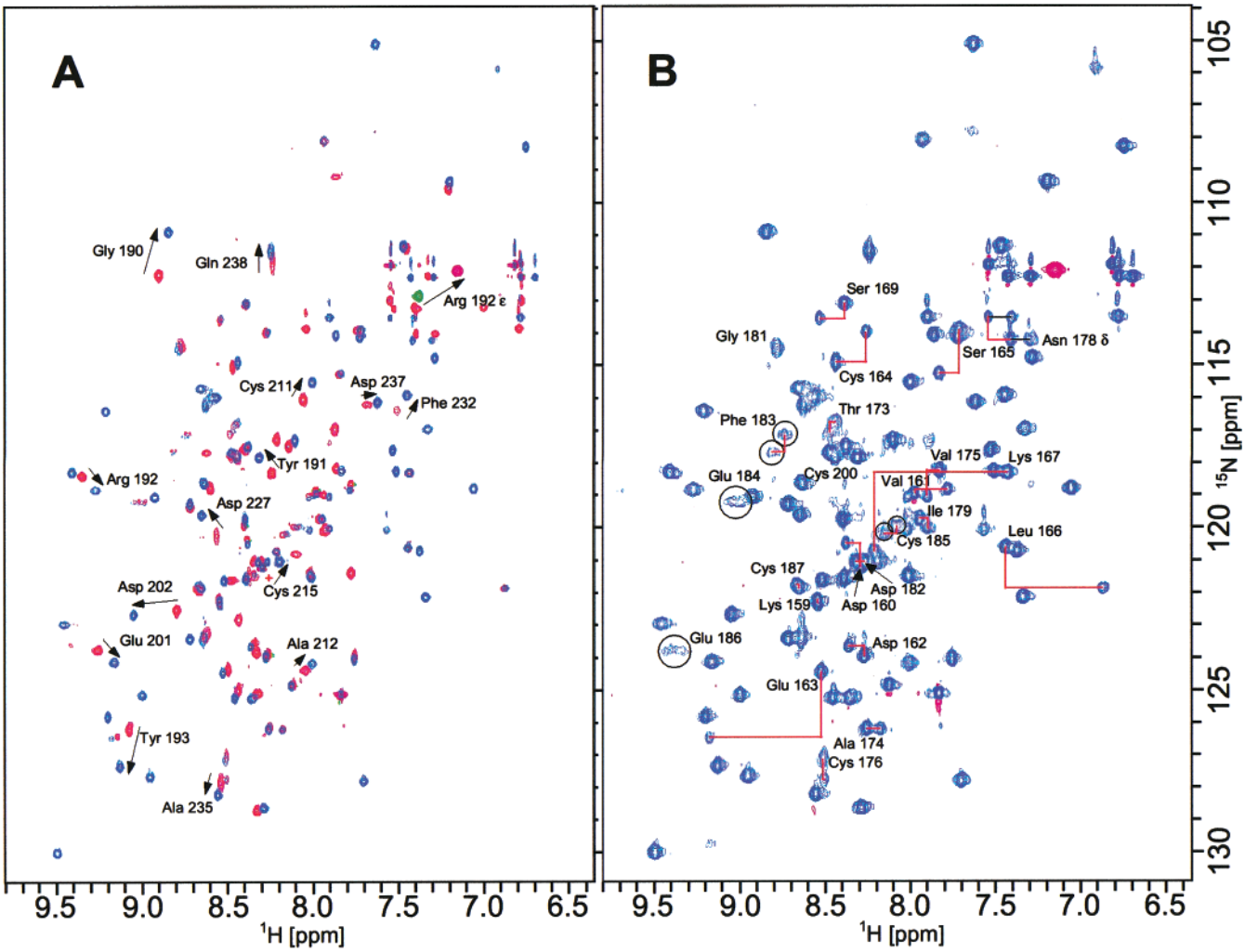

FIGURE 3: (A) Overlay of ^{1}H-^{15}N HSQC spectra of the $(Ca^{2+})_0$ (red) and $(Ca^{2+})_1$ (blue) forms of pS EGF 3-4. The peak from the Arg 192 ϵ group is folded in and is green and magenta in the $(Ca^{2+})_0$ and $(Ca^{2+})_1$ spectrum, respectively. All residues which experience fast-exchange behavior and combined chemical shift changes larger than 0.05 ppm are labeled and arrows indicate how the peaks move when $CaCl_2$ is titrated in. Spectra have been processed to enhance resolution and therefore not all peaks are visible. The position of Cys 215 in the $(Ca^{2+})_0$ state is marked by a (+) sign. (B) ^{1}H-^{15}N HSQC spectrum of the $(Ca^{2+})_1$ form of pS EGF 3-4. Double set components are connected by red lines and the major peaks are labeled. Broadened peaks of Phe 183, Glu 184, Cys 185, and Glu 186 are marked with circles in the spectrum. The two peaks from each set of NH_2 resonances of Asn 178 are connected by black lines. The spectrum has been processed to enhance sensitivity.

No exchange peaks between major and minor forms were observed in either NOESY, ^{1}H-^{15}N NOESY−HSQC (mixing times 80 and 150 ms), or R1EX (exchange delay 738 ms) spectra of pS EGF 3-4 at 36 °C. Attempts to detect exchange peaks at higher temperatures also failed. These experiments were, however, hampered by temperature-dependent increase of both amide proton exchange with solvent and longitudinal relaxation rate (R_1).

The cis−trans isomerization of the peptide bond preceding a proline is a well-known phenomena and short distances $H^N(i)$−Pro $H^\delta(i+1)$ and/or $H^\alpha(i)$−Pro H^δ $(i+1)$ are diagnostic for a trans peptide bond whereas short $H^N(i)$−Pro $H^\alpha(i+1)$ and/or $H^\alpha(i)$−Pro H^α $(i+1)$ distances are characteristic of the cis conformation (*57*). Spectra of pS EGF 3 exhibit a significantly lower degree of spectral overlap as well as narrower lines and were therefore very useful for elucidating the origin of the resonance doubling. In the remainder of this paragraph as well as in Figures 5 and 9, when referring to resonances from the major and minor forms, we will use the three-letter and one-letter codes for amino acids, respectively. For the peptide bond preceding Pro 168, we observed for the major conformation two weak Lys 167 H^N−Pro 168 H^δ and two medium Lys 167 H^α−Pro 168 H^δ NOEs in a 150 ms NOESY spectrum recorded at 10 °C (Figure 5) (Lys 167 H^α is overlapped by the water resonance at 36 °C). This shows that the major form has a trans peptide bond preceding Pro 168. The complementing data for the minor form was more difficult to get at as the K 167 H^α resonance signal at 4.40 ppm was too close to the P 168 H^α frequency at 4.44 ppm. Thus, the K 167 H^α−P 168 H^α cross-peak lies close to the diagonal and is difficult to observe. The K 167 H^α−P 168 H^δ cross-peaks (indicating trans) may be overlapped by intraresidue P 168 H^α−P 168 H^δ cross-peaks, however, no signals are observed at this spectral location, and therefore, it seems appropriate to assume that the minor conformation represents a cis K 167−P 168 peptide bond.

The conclusion, that two conformations exist with the Lys 167−Pro 168 peptide bond in trans and cis for the major and minor forms, respectively, is consistent with location of the double sets of resonances with the largest shift differences

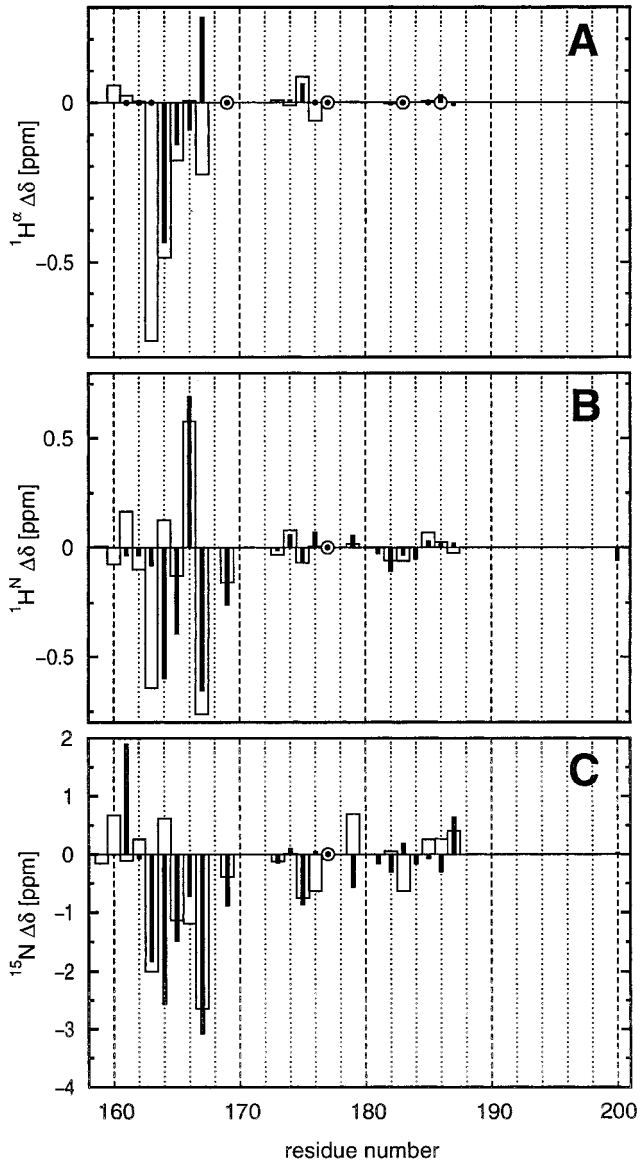

FIGURE 4: Chemical shift difference between major and minor peaks of the same residue in pS EGF 3-4 for $^1H^\alpha$ (A), $^1H^N$ (B), and ^{15}N (C). Shift differences observed in the $(Ca^{2+})_1$ and $(Ca^{2+})_2$ forms are marked by open wide bars and filled narrow bars, respectively. Resonances, which could not be observed in the $(Ca^{2+})_1$ or $(Ca^{2+})_2$ form due to exchange broadening or spectral overlap are represented by large open circles and small filled circles, respectively. No double sets of peaks were found in EGF 4 and therefore only the region comprising EGF 3 is displayed.

between components for residues immediately N-terminal of Pro 168 (Figure 4). Spectroscopic data for the remaining three proline residues in pS EGF 3-4 is consistent with trans peptide bonds, and no evidence for isomerization was found.

Considering the absence of any exchange peaks and the R_1 values [which were measured at 36 °C (see below)] we can estimate that the exchange rate (k_{ex}) for the peptide bond isomerization must be slower than 0.2 s^{-1} at 36 °C (*58*). As the interconversion cannot be demonstrated it is possible that the two sets of peaks arise from two energetically favorable conformations produced during the refolding of the protein. Interconversion rates for proline cis−trans isomerization in proteins have been reported to be in the range 0.03-0.26 s^{-1} measured at different conditions (*59*−*61*). Interestingly, proline cis−trans isomerization taking place on a very slow time scale was recently reported for the TB domain from fibrillin-1 (*62*).

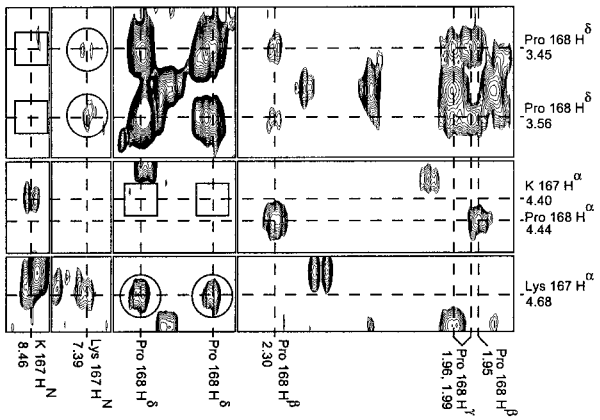

FIGURE 5: Tiles from a 150 ms NOESY spectrum of Ca^{2+}-free pS EGF 3 at 10 °C. Assignments and chemical shifts in ppm are indicated. Lys 167 H^N-Pro 168 H^δ and Lys 167 H^α-Pro 168 H^δ NOE cross-peaks (circles) are observed but not K 167 H^N-P 168 H^δ or K 167 H^α-P 168 H^δ (squares). This indicates that the Lys 167-Pro 168 peptide bond is trans while the K 167-P 168 bond is not.

Ca^{2+} Titration. NMR monitored Ca^{2+} titrations have previously been used to determine the Ca^{2+} affinity of EGF modules using one-dimensional (1D) NMR experiments (*5*, *10*, *13*, *19*, *26*, *63*−*66*) and 2D NOESY experiments (*14*, *15*, *23*). In most cases the $^1H^{\delta/\epsilon}$ shifts of the conserved aromatic residue in the major β-sheet have been monitored. We monitored the Ca^{2+} titration to pS EGF 3-4 employing 2D ^1H-^{15}N HSQC spectra and used the displacement of several cross-peaks to calculate the K_d of the weak-affinity site in EGF 3.

In a previous study, we determined a K_d of 4.8 mM for Ca^{2+} binding to the major conformer in a 0.21 mM sample of pS EGF 3-4 at 27 °C, pH 7.5, in the presence of 150 mM NaCl (*21*). These parameters were chosen to match conditions used in many of the previously reported K_d measurements, allowing a straightforward comparison of Ca^{2+} affinities. In the present study, however, measurements were done on a 1.1 mM sample at 36 °C, pH 6.0, with no addition of salt besides the $CaCl_2$ and a small amount of NaN_3. These conditions were chosen to optimize the conditions for the NMR experiments, and the results can thus be related to the results from forthcoming structural and dynamical studies. Further, to be able to study the effects of Ca^{2+} binding to the high-affinity site in EGF 4, care was taken to produce a Ca^{2+}-free sample. In the earlier study this high-affinity site was saturated at the start of the titration.

The initial binding of Ca^{2+} to pS EGF 3-4 takes place at the high-affinity site in EGF 4 and is characterized by slow to intermediate exchange, on the NMR time scale, between the $(Ca^{2+})_0$ and the $(Ca^{2+})_1$ forms. As shown in Figure 3A, resonances from residues in the vicinity of the Ca^{2+}-binding site broaden and disappear from one location in the spectrum and reappear in a different location. Some other peaks are clearly broadened as a result of exchange on an intermediate time scale. The exchange behavior is dictated by the difference in chemical shift between the two forms. While peaks from 24 residues which are assigned in the $(Ca^{2+})_1$ state disappear at lower Ca^{2+} concentrations, only 10 peaks reappear as narrow signals in the $(Ca^{2+})_0$ state. As these 10

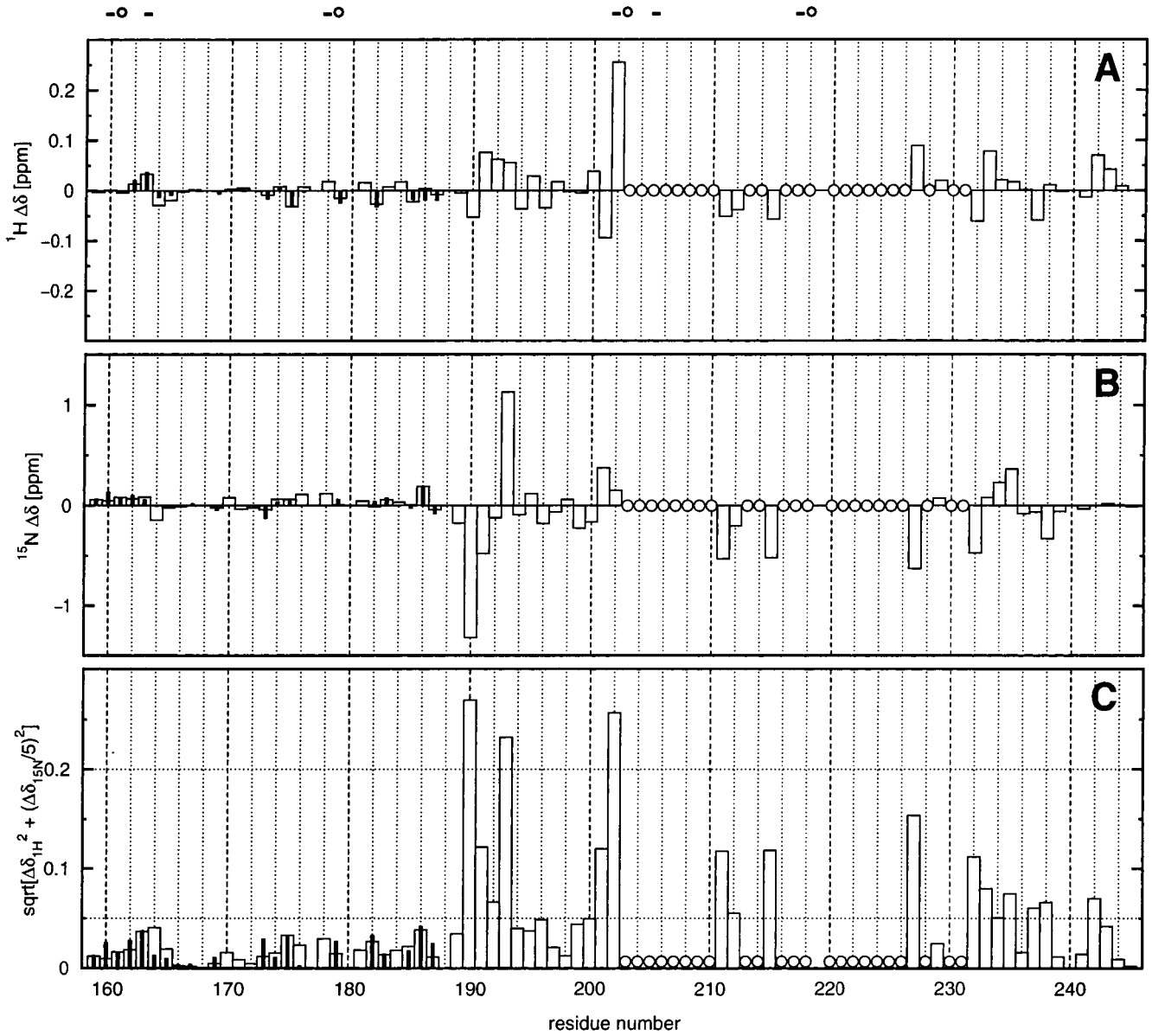

FIGURE 6: Chemical shift differences between the $(Ca^{2+})_1$ and $(Ca^{2+})_0$ forms of pS EGF 3-4. The major set of peaks (open wide bars) and the minor set of peaks (filled narrow bars) for amide protons (A), amide nitrogens (B) and a combination of both ^{1}H and ^{15}N amide chemical shifts calculated as $\Delta\delta_{1H\&15N} = \sqrt{\Delta\delta_{1H}{}^2 + (\Delta\delta_{15N}/5)^2}$ (C). Symbols at the top indicate proposed carboxylate (−) and carbonyl (○) Ca^{2+} ligands. $\Delta\delta_{1H\&15N} > 0.05$ and 0.2 ppm are indicated by a dotted horizontal line. An open circle indicates resonances experiencing slow exchange behavior.

peaks are sharp and the broadening is independent of the chemical shift difference in the limits of slow exchange, it must be concluded that the 14 missing peaks at the onset of the titration are broadened out by an exchange process in the $(Ca^{2+})_0$ state, which is not related to Ca^{2+} binding.

Strong effects from the Ca^{2+} binding, as evidenced by line broadening, are observed for a large number of residues in EGF 4 and involve mostly residues around the Ca^{2+}-binding site and in the major β-sheet (Figures 6 and 7A). A few residues farther from the site are also affected, among them notably Glu 242 in the C-terminal end of pS EGF 3-4, which is barely observable in the spectrum of the $(Ca^{2+})_0$ state. This residue would correspond to the linker, if another EGF module had followed EGF 4. Thus, in addition to Cys 200 discussed above, we have again observed influence from the Ca^{2+} binding in an EGF module on a C-terminal residue. Resonances undergoing shift differences small enough to exhibit fast-exchange behavior can be followed from the $(Ca^{2+})_0$ to the $(Ca^{2+})_1$ state. Sixteen of these resonances exhibit $\Delta\delta_{1H\&15N} > 0.05$ ppm (Figures 6 and 7A) with the largest changes observed for the backbone amide nuclei of Gly 190, Tyr 193, and Asp 202. In addition, the nuclei of the Arg 192 side-chain ϵ-amine group exhibit shift differences in the same range ($\Delta\delta_{1H} = -0.23$ and $\Delta\delta_{15N} = 0.80$ ppm). The large shift change for Asp 202 is not surprising, as it supposedly is a side-chain Ca^{2+} ligand. Gly 190, Arg 192, and Tyr 193 are situated in the last loop of EGF 3, and the intervening Tyr 191 ($\Delta\delta_{1H} = 0.08$ and $\Delta\delta_{15N} = -0.48$ ppm) corresponds to Tyr 2157 in the fibrillin-1 cbEGF 32-33 module pair where it was implicated in an intermodule hydrophobic cluster (*25*). Thus, the large shift changes seen for these nuclei are likely the consequence of a conformational rearrangement resulting from an ordering of structure around the Ca^{2+}-binding site when the ion is bound. The

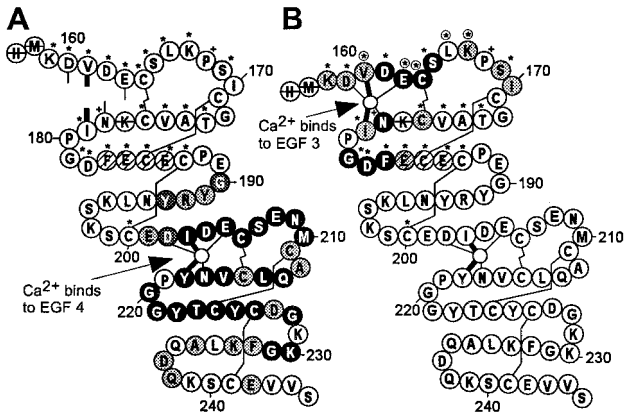

FIGURE 7: Schematic diagram of the pS EGF 3-4 primary structure summarizing backbone amide shift changes resulting from binding of Ca^{2+} to EGF 4 and EGF 3 in panels A and B, respectively. Residues for which double sets of peaks have been found are labeled by (*) backbone and side chain resonances or (+) side chain resonances only. Ca^{2+} ligands are marked as broad lines (backbone ligands) and narrow lines (side-chain ligands). Disulfide bonds are marked as connecting lines. (A) Residues that experience slow exchange between the $(Ca^{2+})_0$ and $(Ca^{2+})_1$ states are labeled as a white character in a black circle, those that experience fast exchange and have $\Delta\delta_{1H\&15N} > 0.2$ ppm are represented by a white character on gray, while those with $0.05 < \Delta\delta_{1H\&15N} < 0.2$ are shown as a black character on gray. (B) Residues that exhibit $\Delta\delta_{1H\&15N} > 0.5$ ppm between the $(Ca^{2+})_1$ and $(Ca^{2+})_2$ states are represented by a black circle, those with $0.125 < \Delta\delta_{1H\&15N} < 0.5$ ppm by a gray circle. Residues with the largest shift difference between resonances of the major and minor forms in either the $(Ca^{2+})_1$ or $(Ca^{2+})_2$ state are labeled by an encircled asterisk ($|\Delta\delta_{H\alpha}| > 0.5$ ppm, $|\Delta\delta_{HN}| > 0.5$ ppm, or $|\Delta\delta_{NN}| > 1.5$ ppm). In both panels unassigned residues are marked by a horizontal line. Residues exhibiting strongly broadened ^1H amide resonances are hatched.

rearrangement affects residues that are involved in the intermodule hydrophobic cluster, possibly resulting in a more restricted relative orientation of the two modules when Ca^{2+} is bound. The large shift changes for Gly 190 and Tyr 193 do not necessarily imply that they are the prime components of the hydrophobic cluster in pS EGF 3-4 as it is possible that limited displacement of the aromatic ring of Tyr 191 can cause large shift changes of backbone resonances in neighboring residues.

Binding to the weak Ca^{2+} site is characterized by fast exchange for all residues, implying that shifts can be followed from the $(Ca^{2+})_1$ form to the $(Ca^{2+})_2$ form. For both the major and minor conformer, the largest shift changes are found close to the proposed Ca^{2+}-ligating residues (Figures 7B and 8) near the N-terminus and near the hairpin-turn of the major β-sheet in EGF 3. However, residues in the intervening loop (Cys 164−Cys 176) as well as on the opposite side of the β-sheet also experience substantial shift changes. This is similar to what was reported for EGF 1 from FX (*7*).

The K_d for binding to the weak site was calculated using a simulated annealing algorithm that has proven to be a robust method taking into account the large number of parameters (*35*). As we have now resolved many of the ambiguities caused by peak doubling, we can include a larger number of nuclei for the calculation than the six used in the earlier study and can also determine the K_d for the minor form separately, while in the earlier study, only the major form was investigated (*21*). The selection criteria (defined in Experimental Procedures) for which nuclei to include in the calculation resulted in 17 and 13 residues (each contributing one $^1H^N$ and one ^{15}N nucleus) from the major and minor forms, respectively (Figure 9). The K_d for Ca^{2+} binding to the weak site was determined to 4.6 ± 0.8 and 2.9 ± 0.7 mM for the major and minor forms, respectively. Calculation of the K_d from a weighted average of individually determined K_d values gave the same result (data not shown).

The value obtained for the major conformer in this study is nearly the same as in the earlier investigation ($K_d = 4.8$ mM) even though a lower ionic strength was used in the present study (*21*). However, a similar small effect from ionic strength has been observed also for the isolated EGF 3 module, while the isolated EGF 4 module had a 14-fold higher affinity at low ionic strength (Figure 1) (*10*). This can be explained by the fact that the total charge at and close to the Ca^{2+}-binding site in EGF 3 is −1, compared to −4 for EGF 4. In addition, the proteins themselves contribute to the electrostatic screening, and thus an increase in the protein concentration (1.1 mM here and 0.2 mM in ref *21*) will counteract the decrease in screening resulting from a lower salt concentration in this investigation (*67*).

Backbone Dynamics. We have run a series of experiments to determine the ^{15}N relaxation rate constants for longitudinal (R_1) and transverse (R_2) auto-relaxation, longitudinal (η_z) and transverse (η_{xy}) cross-correlation relaxation, as well as the ^1H-^{15}N steady-state NOE values, using a 0.5 mM ^{15}N-labeled sample of pS EGF 3-4 in the $(Ca^{2+})_1$ state. Resonances from both major and minor forms could be evaluated, although, in general, the minor peaks gave rise to less accurate results. Interestingly, the ^{15}N relaxation properties of the minor conformer mostly agreed with those of the major conformer with regard to all measured parameters (Figure 10). The following discussion will therefore be restricted to the major form.

PS EGF 3-4 has 85 backbone amide groups, but the cross-peaks of the two N-terminal residues originating from the His-tag, His 157, and Met 158, were not visible in the ^1H-^{15}N HSQC experiments, presumably due to rapid amide proton exchange with the solvent. Also the cross-peaks from Lys 177, Tyr 225, and Ser 240 were missing. For the remaining 80 residues relaxation data were obtained.

In the interest of brevity we restrict the discussion to the steady-state NOEs, residue specific correlation times and exchange terms. These parameters give valuable information on the dynamic behavior of pS EGF 3-4. A full report on the results from the ^{15}N relaxation study will be presented elsewhere.

The steady-state NOE (Figure 10A) gives an indication of fast fluctuations (ps−ns). Our data reveal that the four most N-terminal (Lys 159−Asp 162) and two most C-terminal (Val 244−Ser 245) residues of the wild-type sequence have an enhanced flexibility (NOE < 0.5). The remainder of the N-terminal part of EGF 3 up to the fifth cysteine (Cys 187) is less rigid than the rest of the molecule (average NOE = 0.61). A sequence of five residues (Ile 170−Ala 174) is somewhat less flexible (NOE > 0.64) than the surrounding regions. They may be stabilized by interactions with residues in the C-terminal part of EGF 3 in accordance with intramolecular contacts observed in most published structures of EGF modules. The low NOEs in the N-terminal part of EGF 3 are probably related to the absence of a stabilizing Ca^{2+} in the weak-affinity site in EGF 3 (*68*−*70*).

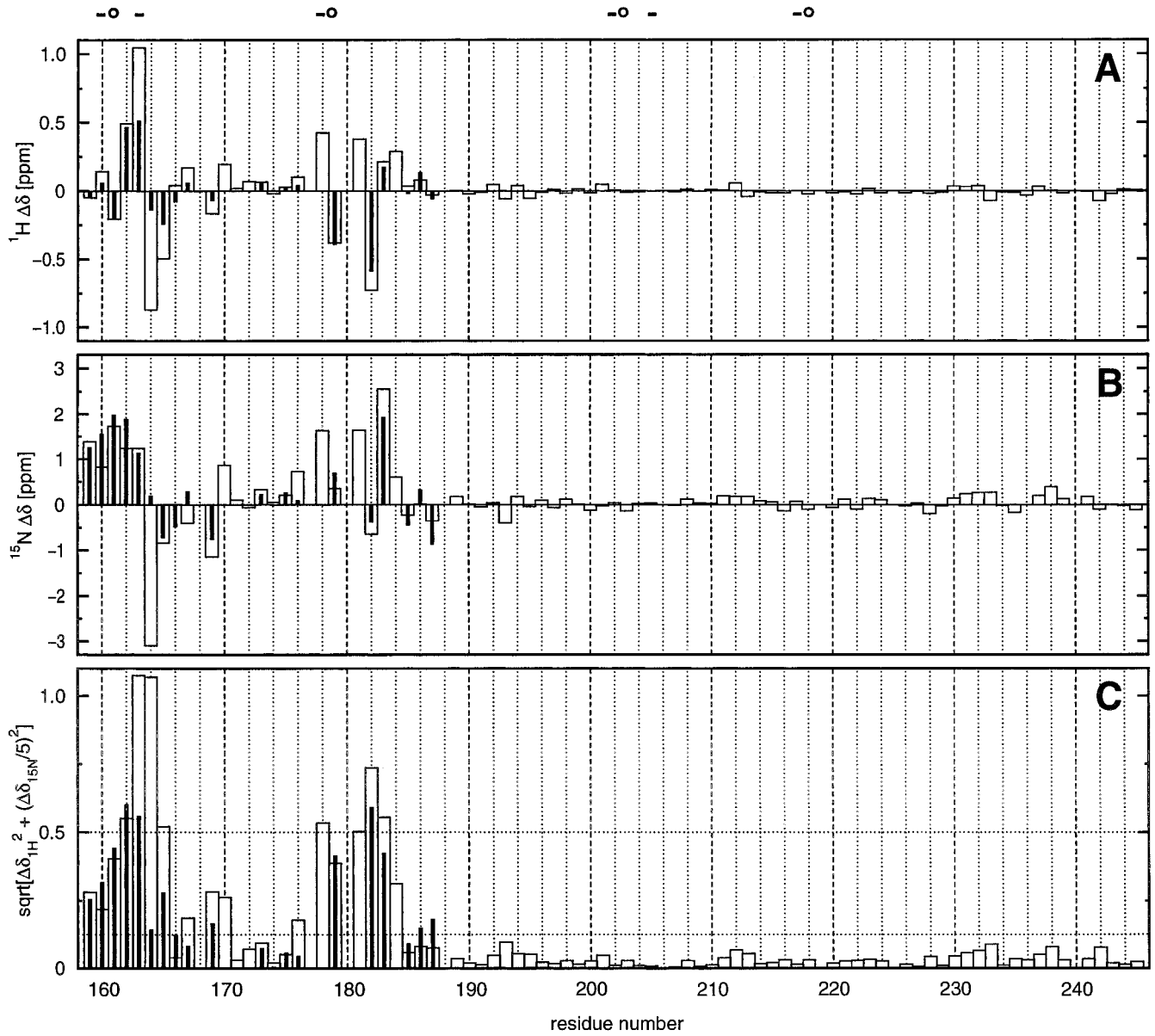

FIGURE 8: Chemical shift differences between $(Ca^{2+})_2$ and $(Ca^{2+})_1$ form of pS EGF 3-4. Symbols according to caption of Figure 6. $\Delta\delta_{1H\&15N} > 0.125$ and 0.5 ppm are indicated by a dotted horizontal line.

The highest NOE values in the protein cluster to three proximal peptide segments (average NOE = 0.75) in the center of the molecule. Two segments, Tyr 191−Leu 195 and Val 216−Tyr 222 enclose residues corresponding to those implicated in the hydrophobic module-module interaction seen in the module pair from fibrillin-1 (*25*). The loop between the fifth and sixth cysteine in EGF 3 is two residues longer than in fibrillin-1 cbEGF 32. As most of the residues in this loop appear to have a rigid backbone, this might indicate a more extensive intermodule interface in pS EGF 3-4. The other segment with high NOE values, Glu 201−Ser 207, is located at the intermodule linker and the N-terminal part of the Ca^{2+}-binding site in EGF 4. Notably, these three rigid segments comprise all residues proposed to ligate Ca^{2+} in the high-affinity site in EGF 4 (Figure 2). The fact that both contact points between EGF 3 and 4, the linker, and the hydrophobic cluster are rigid suggests that the relative orientation between the two modules is well defined, in accordance with the homology to the EGF module pair from fibrillin-1, where this has been demonstrated through structural and dynamical investigations (*25*, *71*).

Anisotropic Rotational Diffusion. Variations in the ratio of transverse and longitudinal relaxation rates (R_2/R_1) may be caused by contributions from chemical exchange or anisotropic rotational diffusion. To circumvent misinterpretation of the relaxation properties of pS EGF 3-4 we measured η_z and η_{xy}, which allowed us to separate chemical exchange contributions from the transverse relaxation rate according to either eq 8 or eq 9, yielding the exchange-free transverse relaxation rate, $R_{2,0}$ (*41*). Calculations of $R_{2,0}$ employing eq 8 have been used to evaluate the backbone dynamics of C-terminal calmodulin domains and were demonstrated to be consistent with other relaxation parameters (*72*, *73*). There is, however, a concern that η_z may be affected by cross-relaxation of the $^1H^N$ nuclei with other ^1H spins, particularly in β-sheet proteins where short $^1H_i^{\alpha}-^1H_{i+1}^{N}$ distances are prevalent. While calmodulin is an α-helical protein, pS EGF 3-4 is a β-sheet protein and consequently more susceptible to this effect. To circumvent this problem, we have devised a method of calculating $R_{2,0}$ independently from η_z (see

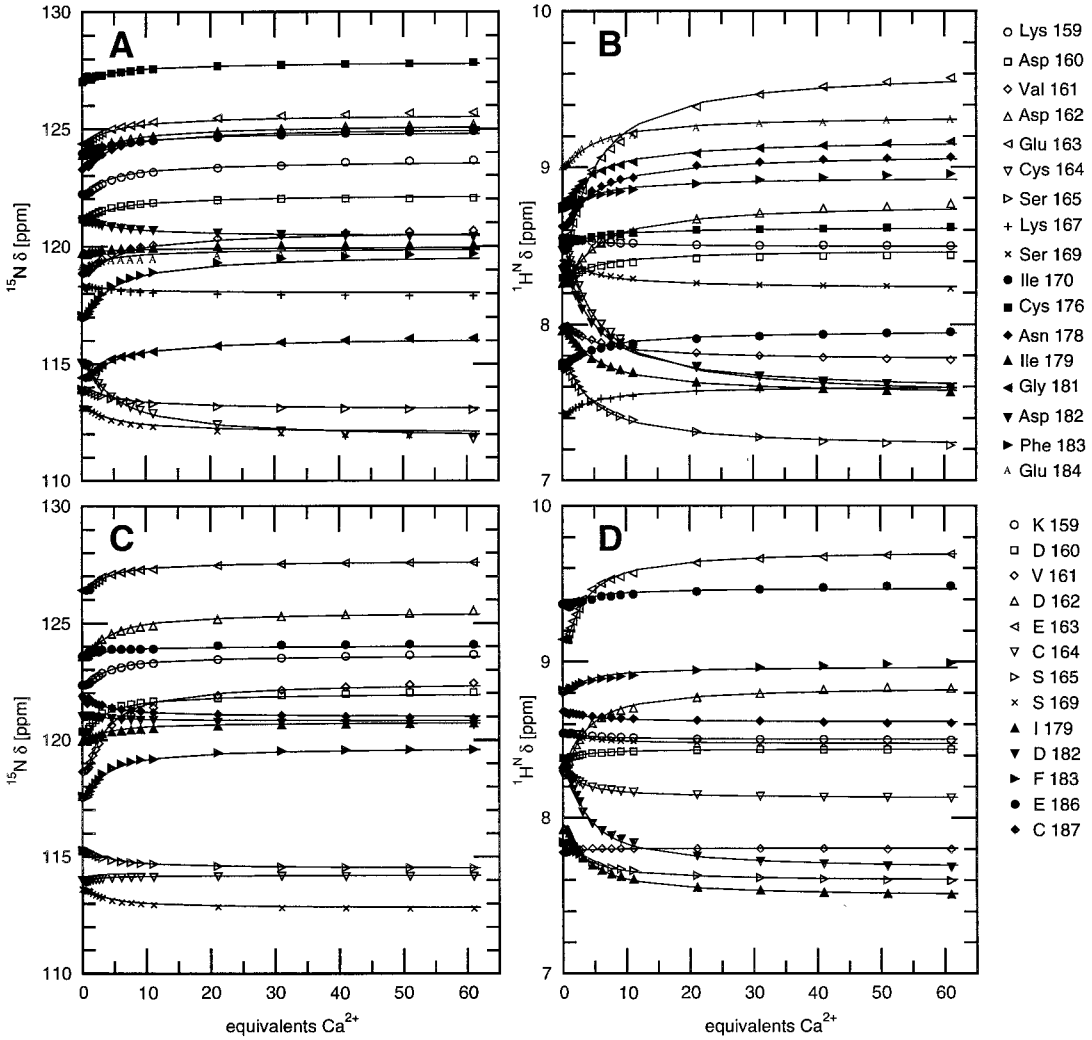

FIGURE 9: Comparison of the agreement between the experimental chemical shifts (symbols according to legend in the figure; three- and one-letter code for amino acids for major and minor peaks, respectively) and calculated chemical shifts (line) during titration of pS EGF 3-4 with $CaCl_2$. Only the ^{15}N (A and C) and ^{1}H (B and D) amide chemical shifts for residues for which $\Delta\delta_{1H\&15N} > 0.125$ ppm were used, and are plotted here for 17 major peaks (panels A and B) and 13 minor peaks (panels C and D). All 60 binding curves fit well to a simple, noncooperative binding model. There are no systematic deviations that might indicate that a more complex binding model would be better.

Experimental Procedures). $R_{2,0}$ rates calculated using eq 9 are comparable to those calculated using eq 8 with the largest differences found for Gly 172 (1.9 s^{-1}) and Gly 220 (1.4 s^{-1}). A detailed quantitative comparison of the two methods will be presented elsewhere.

From the ratio of $R_{2,0}$ and R_1 we have calculated estimates of the residue-specific rotational diffusion correlation times (τ_c) for residues with NOE > 0.65 (Figure 10B) (*41*, *54*, *55*). The weighted average over all residues with NOE > 0.65 is $\tau_c = 6.6 \pm 0.1$ ns, which is higher than that of the fibrillin-1 cbEGF 32-33 module pair ($\tau_c = 5.3-5.7$ ns for protein concentrations of 2−5 mM at 35 °C) (*71*). The difference in τ_c for these homologous proteins may be attributed to partial aggregation of pS EGF 3-4 or a difference in the hydrodynamic properties.

Bond vectors that are oriented parallel to the long axis of the diffusion tensor of the molecule are predominantly affected by the relatively slow rotational diffusion about the short axis of the diffusion tensor and this is reflected in the ^{15}N relaxation rates leading to high τ_c values. Bond vectors oriented perpendicular to the long axis of the diffusion tensor will accordingly have lower τ_c values. Thus, the heterogeneous distribution of the τ_c values is consistent with a significantly anisotropic diffusion tensor of this molecule. To get a better estimate of the extent of anisotropy, we calculated R_1 and R_2 using spectral density functions under the assumption of an axially symmetric diffusion tensor and found the best fit for theoretically calculated ranges of R_1 and R_2 values and the range of R_1 and $R_{2,0}$ values obtained in our experiments for $D_{||}/D_{\perp} \approx 1.5$, where $D_{||}$ and $D_{\perp}$ are the principal elements of an axially symmetric diffusion tensor (see Experimental Procedures). This estimate of $D_{||}/D_{\perp}$ is fairly coarse, and therefore, we feel that it is advisable to use the simplest anisotropy model available, i.e., that of an axially symmetric diffusion tensor. The accurate determination of the diffusion tensor has to await the determination of the tertiary structure. Despite the coarse method, our result agrees surprisingly well with the anisotropy reported for the fibrillin-1 cbEGF 32-33 module pair ($D_{||}/D_{\perp} = 1.55$) for which the tertiary structure is known (*71*).

Chemical Exchange Broadening. In addition to the resonance doubling of certain residues described above, the assignment process was hampered by severe line broadening, primarily affecting several $^{1}H^{N}$ resonances in the major

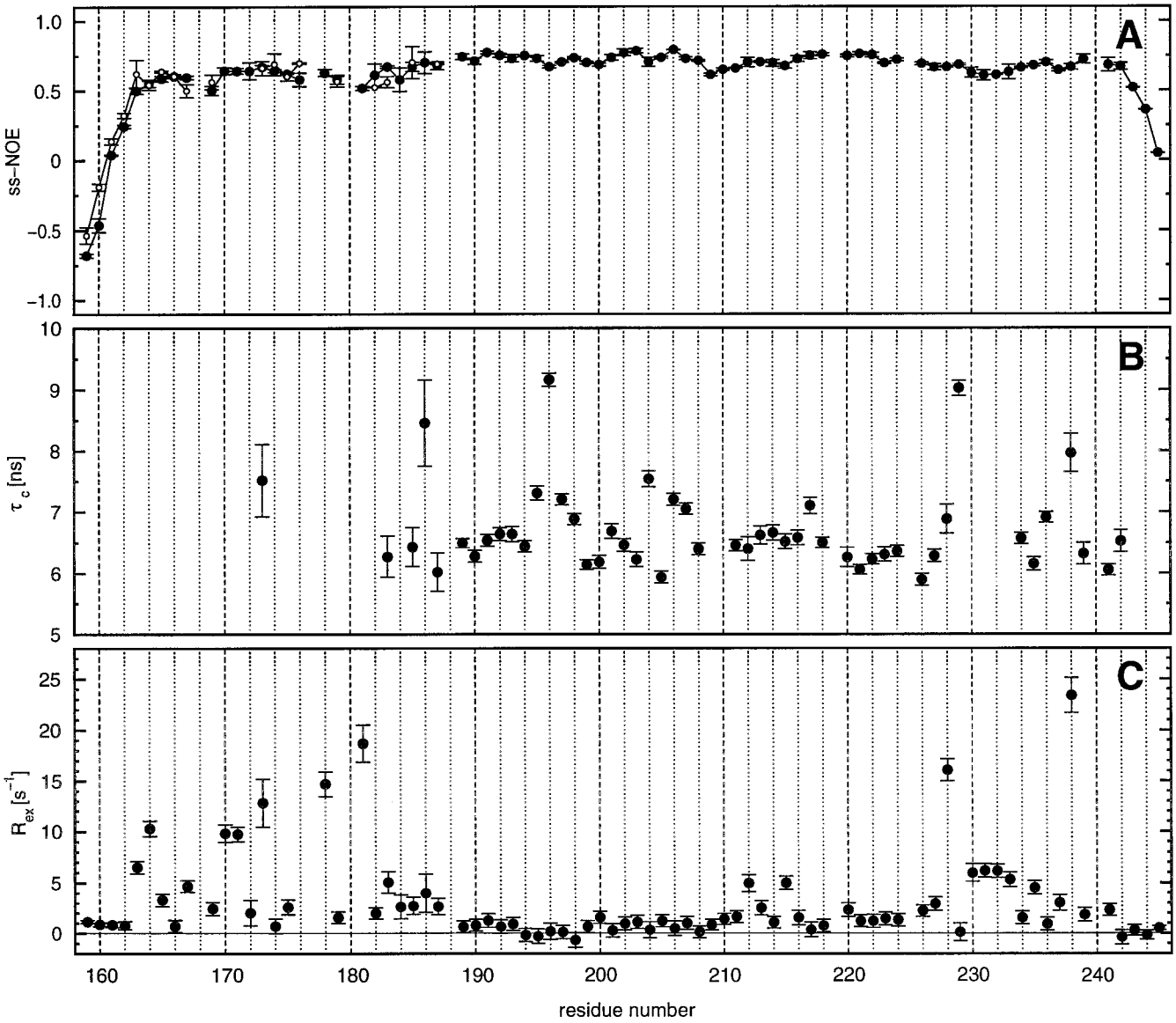

FIGURE 10: Results from ^{15}N spin relaxation experiments. Filled and open circles represent data from the major and minor conformers, respectively. (A) Steady-state {^{1}H}-^{15}N NOE. (B) Residue-specific correlation times (τ_c) calculated from $R_{2,0}/R_1$, where $R_{2,0}$ is the exchange-free ^{15}N transverse relaxation rate (see Experimental Procedures). Only results for residues which have a steady-state NOE > 0.65 have been included. (C) Residue-specific chemical exchange contributions, $R_{ex} = R_2 - R_{2,0}$.

β-sheet of EGF 3. This region was therefore difficult to assign, as many of the critical scalar cross-peaks as well as many NOEs were very weak or missing. When more Ca^{2+} was titrated in, i.e., going from the $(Ca^{2+})_1$ to $(Ca^{2+})_2$ state, the broadening was somewhat reduced and many more diagnostic NOE cross-peaks were available in the ^{1}H-^{15}N NOESY−HSQC spectrum. The most severely affected spin systems were finally assigned to the four-residue stretch Phe 183−Glu 186 (Figures 3B and 7). This effect persists in the isolated EGF 3 module. Thus, an influence of EGF 4 on chemical exchange broadening in EGF 3 can be excluded.

By calculating residue-specific chemical exchange contributions, $R_{ex} = R_2 - R_{2,0}$, processes on a microsecond to millisecond time scale were demonstrated. These motions are predominantly observed for residues in the N-terminal region (Figure 10C). Relative populations of 1, 99, and 0% of pS EGF 3-4 for zero, one, and two Ca^{2+} bound, respectively, were calculated from the K_ds and the known protein and Ca^{2+} concentrations in the sample. The broadening could potentially arise from exchange between the $(Ca^{2+})_1$ state and either of the other states [most likely the $(Ca^{2+})_2$ state as the most affected resonances are close to the weak-affinity site in EGF 3] but due to the low occupancy of both the $(Ca^{2+})_0$ and the $(Ca^{2+})_2$ states this seems unlikely. We calculated the exchange contribution from this process using eq 11. Taking Phe 183 ^{15}N as an example [$\delta\nu = 156$ Hz, assuming diffusion-controlled binding; $k_{on} = 10^9$ $M^{-1}s^{-1}$; $k_{off} = k_{on}K_d = 4.6 \times 10^6$ s^{-1}] we obtained a contribution $\Delta\nu_{1/2} = 1 \times 10^{-4}$ Hz, i.e., negligible in relation to $\Delta\nu_{1/2,exp} = R_{ex}/\pi = 1.9$ Hz for this residue. However, as the broadening decreased somewhat upon Ca^{2+} binding, it is clear that the status of the Ca^{2+} occupancy in EGF 3 is of some importance for this phenomenon. Nevertheless, calculations indicate that the observed exchange terms are mainly governed by processes other than the Ca^{2+} exchange between the $(Ca^{2+})_1$ and $(Ca^{2+})_2$ states. This conclusion is further strengthened considering that exchange broadening for many resonances persists in a Ca^{2+}-saturated sample, in

which the $(Ca^{2+})_2$ state is populated to approximately 93%, while several resonances, exhibiting shift changes of the same magnitude upon Ca^{2+} binding, do not exhibit any exchange contributions. A possibility that has to be taken into consideration is that exchange between monomer and dimer or multimolecular aggregates may cause line broadening. It was recently demonstrated that residues located in the interfacial region of a homodimer with weak affinity of rat CD2d1 were exchange-broadened (*74*). Another explanation for the extensive exchange broadening is that certain regions of pS EGF 3-4 have more conformational freedom. For the N-terminal part of the fibrillin-1 cbEGF 32-33 module pair, Werner et al. also reported exchange broadening of similar magnitude and distribution (*71*). However, the two residues exhibiting large R_{ex} terms in the C-terminus, Gly 228 (R_{ex} = 16.1 s^{-1}) and Gln 238 (R_{ex} = 23.4 s^{-1}), have no counterpart in the fibrillin structure. These two residues are both in locations of the sequence with limited similarity between pS EGF 3-4 and fibrillin-1 cbEGF 32-33 (Figure 2). Werner et al. suggested that the lower Ca^{2+} affinity of the N-terminal site was a consequence of dynamics in the microsecond to millisecond time scale, leading to a less well determined binding site. The existence of a correlation between slow dynamics and Ca^{2+} affinity is possible as for both module pairs the line broadening is somewhat, but not completely, reduced upon saturation of the low-affinity Ca^{2+}-binding site. The module−module interaction with a preceding EGF module might lead to a decrease of slow dynamics around the Ca^{2+}-binding site resulting in a considerably higher Ca^{2+} affinity.

DISCUSSION

We have investigated pS EGF 3-4 as well as pS EGF 3 using a variety of NMR methods. The effect of Ca^{2+} binding was studied, and dynamic processes on three distinct time scales differing by several orders of magnitude were discovered.

We observed extensive effects from Ca^{2+} binding. In particular, the binding to the high-affinity site in EGF 4 affected a majority of resonances in EGF 4 as well as resonances from residues in EGF 3 that participate in intermodule contacts. This demonstrates the importance of Ca^{2+} for structural integrity and module−module interactions in protein S. For both modules, it was noted that Ca^{2+} binding to the sites located in the N-terminal half of each module caused chemical shift effects on resonances from C-terminal residues of that module. This may implicate "communication" in protein S between the Ca^{2+}-binding site in one of the EGF modules and the succeeding module. Such an interaction may be related to the observation that not only the addition of an EGF module N-terminally, but also C-terminally can modulate the Ca^{2+} binding affinity of the EGF modules of protein S (Figure 1) (*65*). The dependence of K_d on the addition of a module C-terminally has so far only been observed in protein S.

The presence of two isoforms, characterized by a cis or trans Lys 167−Pro 168 peptide bond, is visualized by resonance heterogeneity in the N-terminal module. The two conformers do not convert on time scales that were accessible to the experiments (k_{ex} < 0.2 s^{-1}). Both conformers bind Ca^{2+} with similar affinities; K_d values of 4.6 ± 0.8 and 2.9 ± 0.7 mM were obtained for the major and minor forms, respectively. The resonance heterogeneity is independent of the presence of EGF 4. The effect of EGF 2 on the structure of EGF 3 in the intact protein remains to be investigated, and it is uncertain whether both conformations are populated to an appreciable extent.

In addition, chemical exchange on a microsecond to millisecond time-scale is present for a number of residues in the N-terminal part of EGF 3 as evidenced by line broadening and exchange contributions detected by ^{15}N spin relaxation experiments. The line broadening persists in pS EGF 3. The reason for this exchange has not been established, but we have noted that the extent of line broadening decreases when Ca^{2+} is bound at the site in EGF 3. Nevertheless, significant broadening due to exchange between the $(Ca^{2+})_1$ and $(Ca^{2+})_2$ states can be excluded. Exchange between monomer and dimer or increased conformational freedom in certain regions of the protein are likely explanations. Slow dynamics of similar extent was reported for the N-terminal module of fibrillin-1 cbEGF 32-33, thus, it might be a general feature for the most N-terminal module in tandem repeats of EGF modules. In the $(Ca^{2+})_0$ state, several resonances in EGF 4 are broadened out as a consequence of an exchange process that is not related to Ca^{2+} binding. The observations in pS EGF 3-4 of exchange processes in EGF 3 as well as exchange processes in EGF 4 when this module is devoid of Ca^{2+} are consistent with the idea that the presence of an N-terminally neighboring EGF module gives the structural stability that is necessary for preformation of a rigid Ca^{2+}-binding site, which seems to be a prerequisite for high-affinity Ca^{2+} binding. In such a case, the negative effect of entropy loss upon ordering of the Ca^{2+}-binding site upon binding is avoided. The structural stability is further improved by Ca^{2+} binding, as demonstrated by the absence of exchange terms around the Ca^{2+}-binding site in EGF 4 in the Ca^{2+}-bound form of pS EGF 3-4.

Further, steady-state NOE data indicate a significant amount of flexibility on a picosecond to nanosecond time-scale in the N-terminal region of EGF 3, which may be explained by the absence of a Ca^{2+} ion in the weak binding site, as has been demonstrated for other Ca^{2+}-binding proteins (*68*−*70*). In addition, the steady-state NOE data delineate three regions with a rigid backbone. These regions are associated with the linker, the high-affinity Ca^{2+}-binding site in EGF 4, and the extended region around residues corresponding to those involved in the intermodule hydrophobic cluster found in the structure of fibrillin-1 cbEGF 32-33 (*25*). All residues constituting the intermodule contacts are rigid, which implies that the relative orientation of the two modules of pS EGF 3-4 is well determined when the high-affinity Ca^{2+}-binding site is occupied.

The apparent correlation time deduced from $R_{2,0}/R_1$ ratios measured at a protein concentration of 0.5 mM of 6.6 ns is slightly higher than that reported for fibrillin-1 cbEGF 32-33 (5.3−5.7 ns). The difference in τ_c for these homologous proteins may be attributed to partial aggregation of pS EGF 3-4 or a difference in the hydrodynamic properties. A tendency to aggregate would not be a surprising property of modules that play an important role in protein−protein interaction. It has been shown that protein S binds to FXa and that EGF modules 3−4 are crucial for this interaction

(*21*, *75*). The extent of the binding interface remains to be determined. Recently, Pauls et al. showed, using analytical ultracentrifugation, that intact protein S reversibly self-associates in the absence of Ca^{2+} but behaves like a monomer in the presence of high concentrations of Ca^{2+} like in blood ($[Ca^{2+}] \approx 1.2$ mM) (*76*). The transition midpoint was at 0.42 mM Ca^{2+}, which indicates that the low-affinity sites in the Gla module ($K_d \approx$ mM) are determinat of this behavior. The difficulty of removing Ca^{2+} from the high-affinity sites in intact protein S is well documented (*8*). Consequently, it is likely that the high-affinity Ca^{2+}-binding sites in the EGF modules remain saturated and are not involved in the regulation of the self-association reported by Pauls et al. (*76*).

Estimates of residue-specific τ_c values suggest a significantly anisotropic rotational diffusion tensor. Comparison of the dispersion of experimental R_1 and $R_{2,0}$ with R_1 and R_2 calculated from spectral density functions assuming an axially symmetric diffusion tensor suggest a $D_{||}/D_{\perp}$ of approximately 1.5.

ACKNOWLEDGMENT

We thank Eva Thulin (Physical Chemistry 2) for protein expression, Christina Steen (Clinical Chemistry) for assistance with expression and purification of pS EGF 3-4, and Ingrid Dahlquist (Clinical Chemistry) for synthesizing EGF 3. Mikael Akke (Physical Chemistry 2) is acknowledged for valuable discussions and for providing several scripts and macros that have been useful in the data analysis.

REFERENCES

1. Dahlbäck, B. (1995) *Thromb. Res. 77*, 1−43.
2. Lundwall, A., Dackowski, W., Cohen, E., Shaffer, M., Mahr, A., Dahlbäck, B., Stenflo, J., and Wydro, R. (1986) *Proc. Natl. Acad. Sci. U.S.A. 83*, 6716−20.
3. Dahlbäck, B., Lundwall, A., and Stenflo, J. (1986) *J. Biol. Chem. 261*, 5111−5.
4. Long, G. L., Lu, D., Xie, R. L., and Kalafatis, M. (1998) *J. Biol. Chem. 273*, 11521−6.
5. Handford, P. A., Mayhew, M., Baron, M., Winship, P. R., Campbell, I. D., and Brownlee, G. G. (1991) *Nature 351*, 164−7.
6. Mayhew, M., Handford, P., Baron, M., Tse, A., Campbell, I., and Brownlee, G. (1992) *Protein Eng. 5*, 489−94.
7. Selander-Sunnerhagen, M., Ullner, M., Persson, E., Teleman, O., Stenflo, J., and Drakenberg, T. (1992) *J. Biol. Chem. 267*, 19642−9.
8. Dahlbäck, B., Hildebrand, B., and Linse, S. (1990) *J. Biol. Chem. 265*, 18481−9.
9. Gandrille, S., Borgel, D., Ireland, H., Lane, D. A., Simmonds, R., Reitsma, P. H., Mannhalter, C., Pabinger, I., Saito, H., Suzuki, K., Formstone, C., Cooper, D. N., Espinosa, Y., Sala, N., Bernardi, F., and Aiach, M. (1997) *Thromb. Haemost. 77*, 1201−14.
10. Stenberg, Y., Julenius, K., Dahlqvist, I., Drakenberg, T., and Stenflo, J. (1997) *Eur. J. Biochem. 248*, 163−70.
11. Stenberg, Y., Drakenberg, T., Dahlbäck, B., and Stenflo, J. (1998) *Eur. J. Biochem. 251*, 558−64.
12. Persson, K. E., Astermark, J., Björk, I., and Stenflo, J. (1998) *FEBS Lett. 421*, 100−4.
13. Valcare, C., Selander-Sunnerhagen, M., Tämlitz, A.-M., Drakenberg, T., Björk, I., and Stenflo, J. (1993) *J. Biol. Chem. 268*, 26673−26678.
14. Smallridge, R. S., Whiteman, P., Doering, K., Handford, P. A., and Downing, A. K. (1999) *J. Mol. Biol. 286*, 661−668.
15. Knott, V., Downing, A. K., Cardy, C. M., and Handford, P. (1996) *J. Mol. Biol. 255*, 22−7.
16. Kettle, S., Yuan, X., Grundy, G., Knott, V., Downing, A., and Handford, P. (1999) *J. Mol. Biol. 285*, 1277−87.
17. Handford, P., Downing, A. K., Rao, Z., Hewett, D. R., Sykes, B. C., and Kielty, C. M. (1995) *J. Biol. Chem. 270*, 6751−6.
18. Thielens, N. M., Aude, C. A., Lacroix, M. B., Gagnon, J., and Arlaud, G. J. (1990) *J. Biol. Chem. 265*, 14469−75.
19. Hernandez, J.-F., Bersch, B., Petillot, Y., Gagnon, J., and Arlaud, G. J. (1997) *J. Pept. Res. 49*, 221−31.
20. Thielens, N. M., Enrie, K., Lacroix, M., Jaquinod, M., Hernandez, J. F., Esser, A. F., and Arlaud, G. J. (1999) *J. Biol. Chem. 274*, 9149−59.
21. Stenberg, Y., Muranyi, A., Steen, C., Thulin, E., Drakenberg, T., and Stenflo, J. (1999) *J. Mol. Biol. 293*, 653−65.
22. Rand, M. D., Lindblom, A., Carlson, J., Villoutreix, B. O., and Stenflo, J. (1997) *Protein Sci. 6*, 2059−2071.
23. Whiteman, P., Downing, A. K., Smallridge, R., Winship, P. R., and Handford, P. A. (1998) *J. Biol. Chem. 273*, 7807−13.
24. Linse, S., Brodin, P., Johansson, C., Thulin, E., Grundström, T., and Forsén, S. (1988) *Nature 335*, 651−2.
25. Downing, A. K., Knott, V., Werner, J. M., Cardy, C. M., Campbell, I. D., and Handford, P. A. (1996) *Cell 85*, 597−605.
26. Selander-Sunnerhagen, M., Persson, E., Dahlqvist, I., Drakenberg, T., Stenflo, J., Mayhew, M., Robin, M., Handford, P., Tilley, J. W., Campbell, I. D., and Brownlee, G. G. (1993) *J. Biol. Chem. 268*, 23339−44.
27. Wishart, D. S., Bigam, C. G., Yao, J., Abildgaard, F., Dyson, H. J., Oldfield, E., Markley, J. L., and Sykes, B. D. (1995) *J. Biomol. NMR 6*, 135−40.
28. Bartels, C., Xia, T.-H., Billeter, M., Güntert, P., and Wüthrich, K. (1995) *J. Biomol. NMR 5*, 1−10.
29. Farrow, N. A., Zhang, O., Forman-Kay, J. D., and Kay, L. E. (1994) *J. Biomol. NMR 4*, 727−34.
30. Macura, S., and Ernst, R. R. (1980) *Mol. Phys. 41*, 95−117.
31. Braunschweiler, L., and Ernst, R. R. (1983) *J. Magn. Reson. 53*, 521−8.
32. States, D. J., Haberkorn, R. A., and Ruben, D. J. (1982) *J. Magn. Reson. 48*, 286−92.
33. Zhang, O., Kay, L. E., Olivier, J. P., and Forman-Kay, J. D. (1994) *J. Biomol. NMR 4*, 845−58.
34. Grzesiek, S., and Bax, A. (1993) *J. Am. Chem. Soc. 115*, 12593−4.
35. Evenäs, J., Thulin, E., Malmendal, A., Forsén, S., and Carlström, G. (1997) *Biochemistry 36*, 3448−57.
36. Cavanagh, J., Palmer, A. G., Wright, P. E., and Rance, M. (1991) *J. Magn. Reson. 91*, 429−36.
37. Palmer, A. G., Cavanagh, J., Wright, P. E., and Rance, M. (1991) *J. Magn. Reson. 93*, 151−70.
38. Kay, L. E., Keifer, P., and Saarinen, T. (1992) *J. Am. Chem. Soc. 114*, 10663−5.
39. Farrow, N. A., Muhandiram, R., Singer, A. U., Pascal, S. M., Kay, C. M., Gish, G., Shoelson, S. E., Pawson, T., Forman-Kay, J. D., and Kay, L. E. (1994) *Biochemistry 33*, 5984−6003.
40. Tjandra, N., Szabo, A., and Bax, A. (1996) *J. Am. Chem. Soc. 118*, 6986−91.
41. Kroenke, C. D., Loria, J. P., Lee, L. K., Rance, M., and Palmer, A. G. (1998) *J. Am. Chem. Soc. 120*, 7905−15.
42. Shaka, A. J., Barker, P. B., and Freeman, R. (1985) *J. Magn. Reson. 64*, 547−52.
43. Boyd, J., Hommel, U., and Campbell, I. D. (1990) *Chem. Phys. Lett. 175*, 477−82.
44. Kay, L. E., Nicholson, L. K., Delagio, F., Bax, A., and Torchia, D. A. (1992) *J. Magn. Reson. 97*, 359−75.
45. Palmer, A. G., Skelton, N. J., Chazin, W. J., Wright, P. E., and Rance, M. (1992) *Mol. Phys. 75*, 699−711.
46. Carr, H. Y., and Purcell, E. M. (1954) *Phys. Rev. 94*, 630−8.
47. Meiboom, S., and Gill, D. (1958) *Rev. Sci. Instrum. 29*, 688−91.
48. Abragam, A. (1961) *Principles of Nuclear Magnetism*, Clarendon Press, Oxford, U.K.
49. Wang, L., Kurochkin, A. V., and Zuiderweg, E. R. P. (2000) *J. Magn. Reson. 144*, 175−85.

50. Kroenke, C. D., Rance, M., and Palmer, A. G. (1999) *J. Am. Chem. Soc. 121*, 10119−25.
51. Fushman, D., Tjandra, N., and Cowburn, D. (1998) *J. Am. Chem. Soc. 120*, 10947−52.
52. Boyd, J., and Redfield, C. (1999) *J. Am. Chem. Soc. 121*.
53. Woessner, D. E. (1962) *J. Chem. Phys. 37*, 647−54.
54. Brüschweiler, R., Liao, X., and Wright, P. E. (1995) *Science 268*, 886−9.
55. Lee, L. K., Rance, M., Chazin, W. J., and Palmer, A. G. (1997) *J. Biomol. NMR 9*, 287−98.
56. Muranyi, A., Evenäs, J., Stenberg, Y., Stenflo, J., and Drakenberg, T. (2000) *FEBS Lett. 475*, 135−8.
57. Wüthrich, K. (1986) *NMR of Proteins and Nucleic Acids*, John Wiley & Sons, Inc., New York.
58. Jeener, J., Meier, B. H., Bachmann, P., and Ernst, R. R. (1979) *J. Chem. Phys. 71*, 4546−53.
59. Kördel, J., Forsén, S., Drakenberg, T., and Chazin, W. J. (1990) *Biochemistry 29*, 4400−9.
60. Kern, D., Drakenberg, T., Wikström, M., Forsén, S., Bang, H., and Fischer, G. (1993) *FEBS Lett. 323*, 198−202.
61. Amodeo, P., Morelli, M. A., and Castiglione Motta, A. (1994) *Biochemistry 33*, 10754−62.
62. Yuan, X., Werner, J., Knott, V., Handford, P., Campbell, I., and Downing, A. (1998) *Protein Sci. 7*, 2127−35.
63. Persson, E., Selander, M., Linse, S., Drakenberg, T., Öhlin, A.-K., and Stenflo, J. (1989) *J. Biol. Chem. 264*, 16897−16904.
64. Handford, P. A., Baron, M., Mayhew, M., Willis, A., Beesley, T., Brownlee, G. G., and Campbell, I. D. (1990) *EMBO J. 9*, 475−80.
65. Stenberg, Y., Linse, S., Drakenberg, T., and Stenflo, J. (1997) *J. Biol. Chem. 272*, 23255−60.
66. Kao, Y.-H., Lee, G. F., Wang, Y., Starovasnik, M. A., Kelley, R. F., Spellman, M. W., and Lerner, L. (1999) *Biochemistry 38*, 7097−110.
67. Linse, S., Jönsson, B., and Chazin, W. J. (1995) *Proc. Natl. Acad. Sci. U.S.A. 92*, 4748−52.
68. Akke, M., Skelton, N. J., Kördel, J., Palmer, A. G., and Chazin, W. J. (1993) *Biochemistry 32*, 9832−9844.
69. Barbato, G., Ikura, M., Kay, L. E., Pastor, R. W., and Bax, A. (1992) *Biochemistry 31*, 5269−78.
70. Tjandra, N., Kuboniwa, H., Ren, H., and Bax, A. (1995) *Eur. J. Biochem. 230*, 1014−24.
71. Werner, J. M., Knott, V., Handford, P. A., Campbell, I. D., and Downing, A. K. (2000) *J. Mol. Biol. 296*, 1065−78.
72. Evenäs, J., Forsén, S., Malmendal, A., and Akke, M. (1999) *J. Mol. Biol. 289*, 603−17.
73. Malmendal, A., Evenäs, J., Forsén, S., and Akke, M. (1999) *J. Mol. Biol. 293*, 883−99.
74. Pfuhl, M., Chen, H. A., Kristensen, S. M., and Driscoll, P. C. (1999) *J. Biomol. NMR 14*, 307−20.
75. Heeb, M. J., Rosing, J., Bakker, H. M., Fernandez, J. A., Tans, G., and Griffin, J. H. (1994) *Proc. Natl. Acad. Sci. U.S.A. 91*, 2728−32.
76. Pauls, J. E. D., Hockin, M. F., Long, G. L., and Mann, K. G. (2000) *Biochemistry 39*, 5468−73.

BI0004450